

A permanent magnetic film atom chip for Bose-Einstein condensation

B. V. Hall, S. Whitlock, F. Schamberger, P. Hannaford and
A. Sidorov

ARC Centre of Excellence for Quantum Atom Optics and Centre for Atom Optics
and Ultrafast Spectroscopy, Swinburne University of Technology, Hawthorn, Victoria
3122, Australia

E-mail: brhall@groupwise.swin.edu.au

Abstract.

We present a hybrid atom chip which combines a permanent magnetic film with a microfabricated current-carrying structure used to realize a Bose-Einstein condensate. A novel TbGdFeCo material with large perpendicular magnetization has been tailored to allow small scale, stable magnetic potentials for ultracold atoms. We are able to produce ^{87}Rb Bose-Einstein condensates in a magnetic trap based on either the permanent magnetic film or the current-carrying structure. Using the condensate as a magnetic field probe we perform cold atom magnetometry to probe both the field magnitude and gradient as a function of distance from the magnetic film surface. Finally we discuss future directions for our permanent magnetic film atom chip.

PACS number: 39.90.+d, 03.75.Be, 39.25.+k, 07.55.-w

1. Introduction

A recent technological advance in the area of quantum degenerate gases has been the development of the 'atom chip'. These devices exploit tightly confining, magnetic potentials, created by low power current-carrying wires to simplify the production of Bose-Einstein condensates [1, 2]. In addition, they provide the freedom to realize intricate magnetic potentials with features of size comparable to the atomic de Broglie wavelength. Atom chips have been used to realize atomic waveguides and transport devices for Bose-Einstein condensates [3, 4]. These tools allow controllable manipulation of ultracold neutral atoms, with potential applications in quantum information processing [5, 6] and atom interferometry [7, 8].

For current-carrying wire-based atom chips, technical limitations are imposed by current noise and spatial fluctuations in the current density leading to increased heating rates and fragmentation of cold clouds [9, 10]. In addition, near-field thermal noise in conductors is responsible for a fundamental atom loss mechanism [11]. Atom chips

by Present address: Institut für Quantenoptik, Universität Hannover, 30167 Hannover, Germany

incorporating permanent magnetic materials are expected to overcome many of these difficulties. These materials offer the possibility of ultra-stable magnetic potentials due to their intrinsically low magnetic field noise. Moreover permanent magnetic films are thin and relatively high in resistance compared to current-carrying wires, properties which strongly suppress thermal magnetic field noise [12]. Permanent magnetic materials with in-plane magnetization have recently been used to demonstrate trapping of cold atoms [13] and to produce BEC on a magnetic videotape [14, 15]. Here we employ a novel magnetic material with perpendicular anisotropy, developed specifically for applications with ultracold atoms. Perpendicularly magnetized materials allow arbitrary 2D patterns to be written in the plane of the film and provide magnetic field configurations analogous to those produced by planar microfabricated wires [16, 17].

In this paper we report the realization of a permanent magnetic film/machined conductor atom chip which has been used to produce a ^{87}Rb Bose-Einstein condensate (BEC). In section 2 we present a simple model for a thin film of perpendicularly magnetized material which results in straightforward equations for the magnetic field near the edge of the film. We then describe the principle of trapping ultracold atoms in the potential formed by the permanent magnetic film (the film trap). TbGdFeCo materials are then introduced in section 3 with a description of the deposition process. We measured the bulk properties of the magnetic film using both a superconducting quantum interference device (SQUID) and a magnetic force microscope (MFM). Section 4 describes the construction of the ultra high vacuum (UHV) compatible atom chip. This includes a current-carrying structure to provide time dependent control of surface based potentials and is used to form a conductor-based magnetic trap (the wire trap).

The apparatus and experimental procedures used for making a BEC independently with the film trap or the wire trap are described in section 5. In section 6 we apply the BEC as a novel ultracold atom magnetometer by measuring the spatial decay of the magnetic field from the film. High precision trap frequency measurements in conjunction with radio frequency output coupling also allow the direct determination of the associated magnetic field gradient. In conclusion we speculate on future directions for our permanent magnetic film atom chip.

2. Simple model of a permanent magnetic film

Consider a semi-infinite rectangular magnet with magnetization M and thickness h (Figure 1). The magnet lies in the xy plane with one edge aligned along the y axis. The magnet is uniformly magnetized in the $+z$ direction and the distance from the film is large with respect to the film thickness ($z \gg h$). The magnetic field and the field gradient directly above the edge can be written as

$$B_{\text{film}} = \frac{\mu_0 h M}{2z} \quad \text{and} \quad B_{\text{film}}^0 = \frac{\mu_0 h M}{2z^2} : \quad (1)$$

These expressions are analogous to those derived using Biot-Savart's law for the magnetic field above an infinitely long and thin current-carrying wire. The similarity

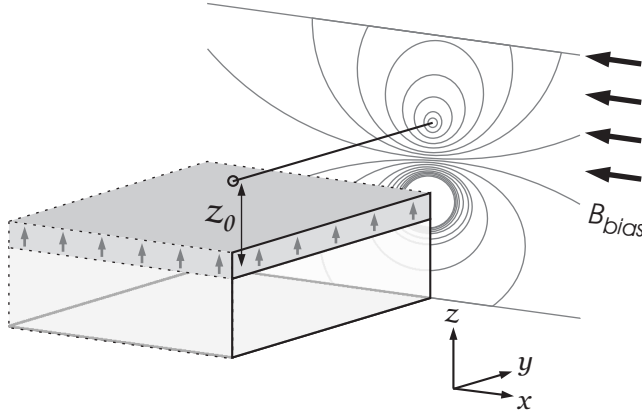


Figure 1. A simple model describes the magnetic field of a semi-infinite, perpendicularly magnetized thin film in combination with a uniform bias magnetic field.

between a permanent magnetic film and a current-carrying wire can be explained using a simple model. An unmagnetized film is comprised of many small magnetic domains of random orientation. The magnetic field produced by each domain is equivalent to that from an imaginary surface current flowing along the domain borders, perpendicular to the magnetization vector [18]. For a uniformly magnetized film with perpendicular anisotropy all domains are aligned in the same direction (out of plane) and within the bulk the magnetic fields of neighbouring domains cancel. A net effective current exists about the perimeter of the film with a magnitude given by the product of the magnetization and the film thickness ($I_{eff} = hM$).

The application of a uniform bias field (B_{bias}) in the x direction produces a radially symmetric two-dimensional quadrupole magnetic field above the film edge at the height z_0 , where the magnitudes of B_{bias} and B_{film} are equal. To realize a three-dimensional (3D) magnetic trap for weak-field seeking atoms a nonuniform axial field B_y is provided by two parallel currents located beneath and perpendicular to the waveguide. Additionally, B_y suppresses spin-flip losses by preventing the total magnetic field at the trap bottom from going to zero. This results in a 3D harmonic film trap at a distance z_0 from the surface with radial frequency given by

$$2 f_{radial} = \frac{1}{2} \frac{hM}{z_0^2} \sqrt{\frac{B_{bias} g_F m_F}{m B_y}}; \quad (2)$$

where B_{bias} is the Bohr magneton, g_F is the Lande factor, m_F is the magnetic quantum number and m is the atomic mass. The ability to produce high quality, thick magnetic films with large magnetization is necessary to produce tightly confining magnetic traps for ultracold atoms.

3. $\text{Tb}_6\text{Gd}_{10}\text{Fe}_{80}\text{Co}_4$ magneto-optical thin films and their properties

The desire for large capacity information storage devices has encouraged an extensive investment toward developing novel magnetic compositions. These are primarily optimized to achieve small scale, recordable patterning of magnetic media. While it is possible to benefit from this experience, applications with cold atoms have several additional yet very specific requirements. Firstly, a high Curie temperature (T_C) will prevent demagnetization during the bake-out procedure, a necessary step in achieving UHV conditions. Secondly, a high coercivity (H_C) will prevent the loss of magnetization when applying large external magnetic fields. Finally, the remanent magnetization (M_R) and the saturation magnetization (M_S) should be large and nearly equivalent, an indication of good magnetic homogeneity. These conditions are satisfied by $\text{Tb}_6\text{Gd}_{10}\text{Fe}_{80}\text{Co}_4$ magneto-optical thin films which have a high Curie temperature ($T_C \approx 300^\circ\text{C}$), perpendicular anisotropy and a square hysteresis loop.

TbGdFeCo thin films were produced using a thin film deposition system (Kurt J Lesker CM S-18) equipped with magnetron sputtering and electron beam evaporation sources [19]. A composite target with a nominal atomic composition of $\text{Tb}_6\text{Gd}_{10}\text{Fe}_{80}\text{Co}_4$ and a high purity chromium target are used in the production of the magnetic thin films. A systematic study of the influence of process parameters over the properties of the thin film indicated that deterioration of the magnetic anisotropy occurs for thin film thickness above 250 nm. In order to maintain good magnetic properties and increase the magnetic field strength near the surface we have implemented a multilayer deposition which produces high quality TbGdFeCo magnetic thin films with a total thickness approaching 1 μm . A glass slide substrate was cleaned in an ultrasonic bath using a nitric acid solution then carefully rinsed before being mounted in the deposition chamber. The base pressure was less than 5×10^{-8} Torr prior to introducing the argon buffer gas ($\approx 4 \text{ mTorr}$). The substrate was then heated to 100°C and a bonding layer of chromium (120 nm) was sputtered on the surface. This was followed by the deposition of six bi-layers of TbGdFeCo (150 nm) and Cr (120 nm) thin films.

The magnetic properties of the multilayer TbGdFeCo/Cr thin film were characterized by a SQUID magnetometer (Figure 2). The hysteresis loop indicates a remanent magnetization of 0.28 T for a total magnet thickness of 900 nm ($\mu_0 M_R = 0.20 \pm 0.01 \text{ A}$). Complete magnetization of the thin film can be achieved by applying a field of 0.8 T, while the thin film magnetization is robust in the presence of external fields below 0.1 T. The surface features of the thin films have also been examined by a high-resolution atomic force microscope operating in magnetic force mode (Figure 3). An unmagnetized sample shows micron-sized features consistent with domain stripes, while an example of a uniformly magnetized sample exhibits excellent magnetic homogeneity.

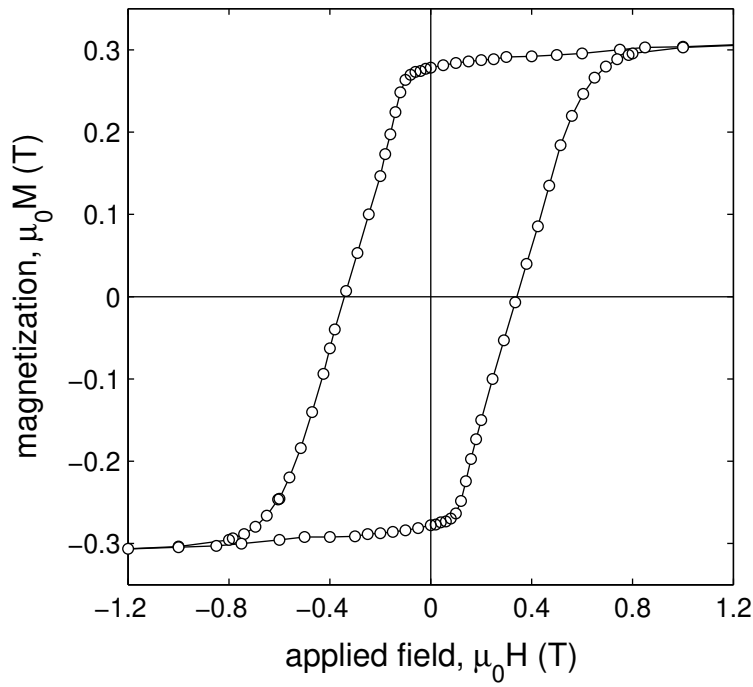


Figure 2. A hysteresis loop derived from SQUID magnetometry of a multilayer $\text{Tb}_6\text{Gd}_{10}\text{Fe}_{80}\text{Co}_4$ magnetic In. The In magnetization is $\mu_0 M_S = \mu_0 M_R = 0.28$ T and the coercivity is $\mu_0 H_C = 0.32$ T.

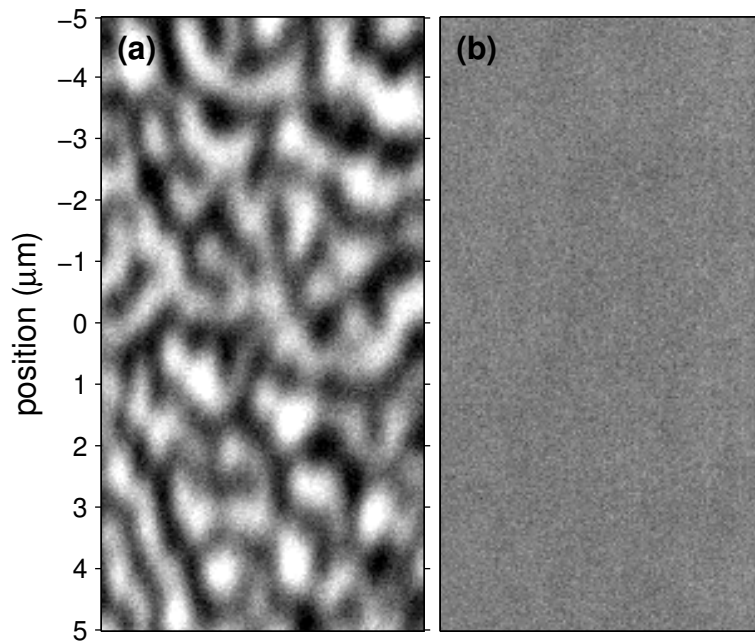


Figure 3. Magnetic Force Microscope (MFM) image of a $\text{Tb}_6\text{Gd}_{10}\text{Fe}_{80}\text{Co}_4$ magnetic In surface. (a) Unmagnetized sample shows domain structure with micron sized features. (b) Uniformly magnetized sample is free of any visible magnetic structure.

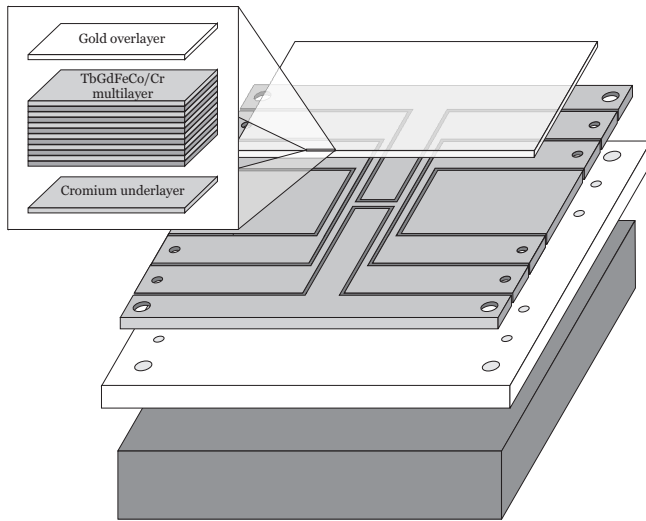


Figure 4. Schematic view of the hybrid atom chip. Inset: TbGdFeCo/Cr multilayer In and Au overlayer. From the top down, glass slide coated with magnetic In, machined silver foil H-wire and end wires, Shapal-M base-plate and Cu heat sink. Missing from the schematic is the second glass slide and two rubidium dispensers

4. Atom chip design

This device represents the first atom chip based on a perpendicularly magnetized permanent magnetic In for trapping ultracold atoms. It has been designed for the production and manipulation of a BEC near the surface of the magnetic material. Although these In's are well suited for making tight and stable trapping potentials up to a few 100 nm from the surface, the small volume of the In trap is not suitable for efficient loading directly from a magneto-optical trap (MOT). To circumvent this difficulty a current-carrying wire structure located beneath the magnetic In provides an additional trapping field. The combination of both the magnetic In and the wire structure represents the hybrid atom chip design shown schematically in Figure 4.

The top layer of the atom chip consists of two adjacent 300 nm thick glass slides which are sturdy enough to prevent warping. The long edges of the glass slides were polished with aluminium oxide grit prior to deposition to remove visible chips. A multilayer TbGdFeCo/Cr In was deposited on one slide using the procedure outlined in Section 3. Both slides were then coated with a gold overlayer (170 nm) and together form a large reflective surface ($40 \times 46 \text{ mm}^2$). This allows the collection of a large number of atoms into a mirror MOT within a single-chamber UHV system. The glass slide coated with the TbGdFeCo/Cr multilayer In was then magnetized in a uniform field of 1 T pending assembly.

The second layer of the hybrid chip is a wire structure which was produced using the micro-machined silver foil technique developed by Vale et al [20]. A 500 nm thick silver foil (99.99 % purity) was fixed with epoxy (Epotek H 77) to a 2 mm thick Shapal-M

machinable ceramic base-plate. A computer controlled Quick Circuit 5000 PCB mill was used to cut 500 μm wide insulating grooves in the foil. Each wire has a width of 1 mm which is broadened to 6 mm far from the trapping region to facilitate good electrical connections. After cutting, the insulating channels were filled with additional epoxy to increase the structural integrity and thermal conductivity. The wire structure including electrical connections has a total resistance of 4.6 m Ω . A continuous current of 30 A can be applied with an associated temperature rise of less than 40 $^{\circ}\text{C}$ and negligible increase in vacuum pressure.

In conventional atom chips U or Z-shape wires are used for creating quadrupole and Ioffe-Pritchard (IP) magnetic field geometries to realize mirror MOTs and magnetic microtraps [21]. In the present atom chip, high currents are used to form a tight trap relatively far from the wire, thereby avoiding unwanted collisions with the surface of the slide. Consequently, the use of broad conductors prohibit the use of separate U and Z-shape wires. This is circumvented with a planar H-shape structure, designed to allow both U and Z-shape current paths with good spatial overlap of the associated traps. Axial confinement for the In trap is provided by additional parallel conductors separated by 9.5 mm and located either side of the H-shape structure. The top surface of the machined silver foil was later polished flat to support the glass slides.

During assembly, the polished edge of the TbGdFeCo In coated slide is aligned to the middle of the H-shape structure and set with epoxy. The second gold-coated slide is epoxied adjacent to the magnetic In slide to complete the reflective chip surface. Two rubidium dispensers are mounted on two ceramic blocks (Macor) which are recessed below the chip surface. The two glass slides, machined silver foil and ceramic base-plate are then fixed to a copper heat sink. The completed chip is clamped to a 19 mm diameter solid copper feedthrough (Ceramaseal, 800 A rating) and mounted in the vacuum chamber. Electrical connections are made using 1.6 mm diameter bare copper wire and BeCu barrel connectors in conjunction with a 12 pin power feedthrough (Ceramaseal, 55 A rating). A cold cathode gauge indicated a pressure below 1×10^{-11} Torr after baking at 140 $^{\circ}\text{C}$ for 4 days, highlighting the UHV compatibility of all materials.

5. Bose-Einstein condensation on a permanent magnetic In

The reflective surface of the atom chip is used to form a mirror MOT and accommodates 30 mm diameter laser beams provided by a high-power diode laser (Toptica DLX 110) locked to the D_2 ($F = 2 \rightarrow 3$) cooling transition of ^{87}Rb . The trapping light is detuned 18 MHz below resonance and has an intensity of 4 mW/cm 2 in each beam. A repumping laser locked to the D_2 ($F = 1 \rightarrow 2$) transition is combined with the trapping light with an intensity of 0.5 mW/cm 2 per beam. Two water-cooled coils mounted outside the vacuum chamber provide a quadrupole magnetic field with gradient 0.1 T/m centered 4.6 mm below the chip surface. To load the mirror MOT a current of 6.5 A is pulsed for 9.5 s through one resistively heated Rb dispenser, allowing the collection of 2×10^8 atoms. The atoms are held for a further 15 s while the UHV pressure recovers, ready for transfer to the chip-based potentials.

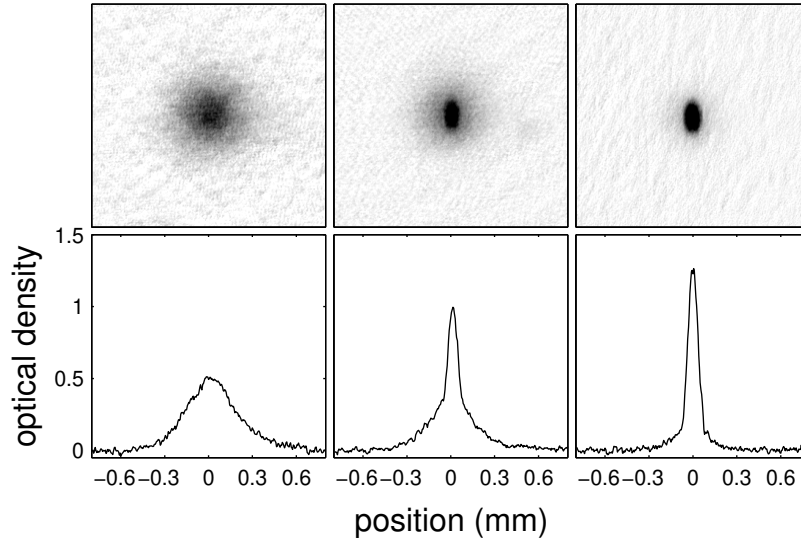


Figure 5. Typical absorption images and optical density profiles of a ballistically expanded atom cloud. Each image is a single realization of the experiment where evaporation is performed in the permanent magnetic In potential. After truncating the evaporation ramp, atoms are held for 150 ms and ballistically expanded for 30 ms before imaging. (a) $RF_{final} = 804$ kHz – thermal cloud, (b) $RF_{final} = 788$ kHz – partially condensed cloud, (c) $RF_{final} = 760$ kHz – an almost pure condensate.

Transfer begins by simultaneously ramping a current through the U-shape circuit ($I_U = 0 \rightarrow 8$ A), increasing the uniform field B_{bias} and turning off the external quadrupole magnetic field over 50 ms. This moves the atoms without loss, into a U-wire MOT located 1.6 mm from the surface and increases the radial gradient to 0.4 T/m. While this compression increases the spatial overlap with the IP potential, it also heats the cloud. To counteract this, the radial gradient is reduced rapidly to 0.11 T/m with the trap light off to minimize any force on the atoms. Polarization gradient cooling is applied for 2 ms with 56 MHz red-detuned trap light to reduce the temperature from 140 K to 40 K. Both the MOT light and I_U are then turned off leaving the cold atoms in a uniform magnetic field.

Next a 200 μ s optical pumping pulse is applied to maximize the number of atoms in the $F = 2; m_F = +2$ weak-field seeking state ready for magnetic trapping. A current (I_Z) of 21.5 A is switched on through the Z-shape circuit while B_{bias} is increased to 1.3 mT to form an IP wire trap at the same position. A total of 4×10^7 atoms are held with a background-limited lifetime greater than 60 s. A diabatic compression of this trap is performed by ramping I_Z up to 31 A and B_{bias} up to 4.0 mT over 100 ms. Further compression results in loss of atoms to the surface. The compressed magnetic trap is 560 μ m from the In surface where the radial and axial trap frequencies are 2×530 Hz and 2×18 Hz respectively. The elastic collision rate in this trap ($\gamma_{el} \approx 50$ s $^{-1}$) is high enough to begin evaporative cooling.

Forced evaporative cooling to the BEC transition begins in the wire trap and is then transferred to the In trap during a single logarithmic radio frequency (RF) ramp. The first 8.85 s of this ramp is a preliminary cooling stage in the wire trap down to a temperature of 5 K. As the cloud is cooled the trap is compressed further to improve the evaporation efficiency by lowering I_z to 25 A, moving the trap to 350 nm from the surface and increasing the radial trap frequency to 2×660 Hz. The RF amplitude is then reduced to zero for 150 ms while the atoms are transferred closer to the chip surface and finally to the In trap. In this trap I_z is zero and axial confinement on the magnetic In edge is provided by the two end wires, each with a current of 6 A. The trap bottom is tuned using an additional magnetic field parallel to the In edge to minimize any discontinuity in the RF evaporation trajectory. The radial and axial trap frequencies are 2×700 Hz and 2×8 Hz respectively. The RF amplitude is then increased again and evaporation continues for 1 s to the BEC phase transition.

Before imaging, the magnetic In trap is adiabatically moved 0.17 mm from the surface to avoid excessive field gradients from the In. The cloud is then released by switching off B_{bias} and the atoms fall under gravity with minor acceleration from the permanent field gradient. Resonant optical absorption is used to image the atoms with a 100 ns⁺ light pulse parallel to the gold surface and tuned to the D_2 ($F = 2 \rightarrow 3$) transition. A CCD camera records the absorption image of the cloud using an achromatic doublet telescope with a resolution of 5 nm/pixel. Using the above procedure a new condensate of $1 - 10^5$ atoms is created every 50 s. Figure 5 shows absorption images and optical density profiles after 30 ms of ballistic expansion. The forced RF evaporation is truncated at 804 kHz, 788 kHz and 760 kHz revealing a thermal cloud, partially condensed cloud and nearly pure condensate, respectively.

It is also possible to form a condensate trapped solely by the wire trap. Here a single, uninterrupted, 10 s RF ramp results in a BEC with atom number comparable to that realized in the In trap. This provides a unique possibility for studying the properties of a BEC in both permanent magnetic and current-carrying trapping environments. In addition, the formation of a BEC independent of the top layer will allow new magnetic structures or materials to be replaced with ease. The wire trap can also be used to transport a BEC to regions on the chip where the magnetic field topology may be different from those near the substrate edge.

6. Magnetic field characterization

The magnetic properties of the TbGdFeCo In were measured prior to mounting on the atom chip using a combination of SQUID and magnetic force microscopy. In-situ techniques using cold atoms have been employed to characterize the magnetic field produced by the In inside the vacuum chamber. This allows a direct comparison with the simple model described earlier. A magnetically trapped cloud of cold atoms or a BEC behaves as an ultra-sensitive probe to the local magnetic field. A measure of the trap position as a function of B_{bias} determines $B_{\text{film}}(z)$, while an independent measure

of the trap frequency is used to determine $B_{\text{film}}^0(z)$.

Once the BEC is confined by the film trap it is possible to probe the magnetic field dependence near the surface. The potential minimum is located at the point where the uniform magnetic field is equal in magnitude to and cancels the field from the film ($B_{\text{bias}} = B_{\text{film}}$). The uniform magnetic field can be increased (decreased) to move the trap minimum closer to (further from) the film surface. The BEC follows the potential minimum and the measurement of cloud position with respect to the film surface determines $B_{\text{film}}(z)$. The strength of B_{bias} is calibrated within the vacuum chamber using untrapped atoms (far from the film) and a short RF pulse resonant with the Zeeman splitting. The pixel size in the imaging plane is calibrated against the gravitational acceleration of freely falling atoms and agrees with the calibration given by imaging a reference rule external to the apparatus. Unfortunately though, the glass substrate coated with magnetic material has recessed approximately 50 μm behind the second blank glass slide as a consequence of unevenly cured epoxy. The exact position of the film surface (in relation to the image) is therefore unknown and presents an uncertainty in $B_{\text{film}}(z)$. For this reason a second technique has been applied to provide more information about the magnetic field from the film.

Harmonic oscillations with small amplitude and frequencies up to 10 kHz can be measured accurately over many periods with a BEC due to low damping rates and small spatial extent. In this case, trap frequencies are measured by exciting radial center of mass motion within the film trap and have been measured to better than 1 Hz ($\sim 0.1\%$ accuracy). These excitations were observed by rapidly increasing the uniform magnetic field by approximately 5% before returning to the original position within 2 to 5 ms. The cloud position was measured after 10 ms of free expansion and data has been taken over five periods of oscillation. In addition, the trap bottom was measured using RF outcoupling with an accuracy better than 10 mG ($\sim 1\%$). The measurement of trap frequency in combination with the trap bottom (B_y) unambiguously determines the local magnetic field gradient (see Equation 2). This combined with the trap position measurements have been used to provide the magnetic field and the magnetic field gradient as a function of height above the surface (Figure 6). This data is consistent with a prediction based on the simple model where the film thickness-magnetization product is given by the prior SQUID measurement ($hM = 0.20 \text{ A}$).

7. Discussion and conclusion

We have demonstrated a hybrid atom chip that exploits perpendicularly magnetized film or current-carrying wires for the production of a BEC. We have developed a multilayer magnetic film structure (TaBdFeCo/Cr) that provides large magnetization and thickness, important for realizing tight and flexible magnetic microtraps. We have used the BEC as a sensitive probe to directly measure the local magnetic field and gradient associated with the magnetic film. These measurements justify the use of the simple model for perpendicularly magnetized magnetic microstructures.

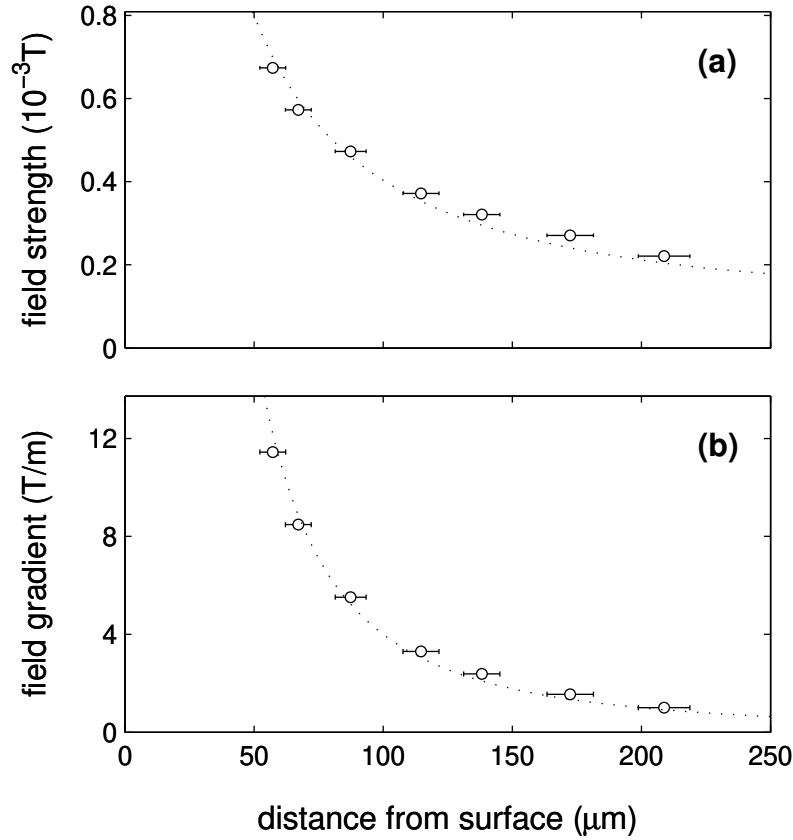


Figure 6. Measurements of the magnetic field strength (a) and field gradient (b) as a function of distance from the surface. The data (open circles) agrees well with predictions (dotted line) of the simple model (see Equation 1). Experimental errors are mostly determined by image resolution and a small uncertainty in the pixel size calibration.

At present we are extending the technique of cold atom magnetometry to the measurement of the spatial dependence of the magnetic field along the thin edge. Spatially dependent magnetic field variations have been observed above microfabricated wire-based atom chips and have been attributed to spatial deviations along the wire edge [10, 22]. Similar phenomena observed in permanent magnetic structures may be caused by substrate roughness, deposition irregularity or ultimately domain reversal. Future studies are aimed at the interaction between a BEC and magnetic thin films. A comparison of the decoherence rates of condensates confined in either the thin or wire-based microtraps may reveal intriguing possibilities for coherent manipulation of cold atoms in microstructured permanent magnetic potentials.

Acknowledgments

We would like to thank J. Wang and D. Gough for carrying out the magnetic thin deposition. This project is supported by the ARC Centre of Excellence for Quantum –

Atom Optics and a Swinburne University Strategic Initiative fund.

References

- [1] Hansel W, Hommelho P, Hansch T W and J Reichel J 2001 Nature 413 498-501
- [2] Ott H, Fortagh J, Schlöterbeck G, Grossmann A and Zimmermann C 2001 Phys. Rev. Lett. 23 230401
- [3] Leinhardt A, Chikkatur A, Kieppinski D, Shin Y, Gustavson T, Ketterle W and Pritchard D 2002 Phys. Rev. Lett. 89 040401
- [4] Müller D, Anderson D Z, Grow R J, Schwindt P D D and Comelle E A 1999 Phys. Rev. Lett. 83 5194
- [5] Calarco T, Hinds E A, Jaksch D, Schmiedmayer J, Cirac J I and Zoller P 1999 Phys. Rev. A 61 022304
- [6] Wang Y-J, Anderson D Z, Bright V M, Comelle E A, Diot Q, Kishimoto T, Prentiss M, Saravanan R A, Segal S R and Wu S 2005 Phys. Rev. Lett. 94 090405
- [7] Shin Y, Sanner C, Jo G-B, Pasquini T A, Saba M, Ketterle W and Pritchard D E 2005 arXiv:cond-mat/0506464
- [8] Schumm T, Hoerberth S, Andersson L M, Wildermuth S, Groth S, Bar-Joseph I, Schmiedmayer J and Krüger P 2005 arXiv:quant-ph/0507047
- [9] Fortagh J, Ott H, Kraft S, Gunther A and Zimmermann C 2002 Phys. Rev. A 66 041604
- [10] Esteve J, Aussibal C, Schumm T, Figl C, Maily D, Bouchoule I, Westbrook C I and Aspect A 2004 Phys. Rev. A 70 043629
- [11] Jones M P A, Vale C J, Sahagun D, Hall B V and Hinds E A 2003 Phys. Rev. Lett. 91 080401
- [12] Scheel S, Rekdal P K, Knight P L and Hinds E A 2005 arXiv:quant-ph/0501149
- [13] Barba I, Gerritsma R, Xing Y T, Goedkoop J B and Spreuw R J C 2005 Eur. Phys. J. D 00055-3
- [14] Sinclair C D J, Curtis E A, Lorente Garcia I, Retter J A, Hall B V, Eriksson S, Sauer B E and Hinds E A 2005 Preprint arXiv:cond-mat/0503619
- [15] Sinclair C D J, Curtis E A, Lorente Garcia I, Retter J A, Hall B V, Eriksson S, Sauer B E and Hinds E A 2005 Preprint arXiv:physics/0502073
- [16] Eriksson S, Ramirez-Martinez F, Curtis E A, Sauer B E, Nutter P W, Hille W and Hinds E A 2004 Appl. Phys. B 79 811
- [17] Jaakkola A, Shevchenko A, Lindfors K, Hautakorpi M, Ilyashenko E, Johansen T H and Kaivola M 2005 Eur. Phys. J. D 00176-7
- [18] Jackson J D 1999 Classical Electrodynamics 3rd Edition (New York: Wiley) chap 5
- [19] Wang J Y, Whitlock S, Schamberger F, Gough D S, Sidorov A I, McLean R J and Hannaford P 2005 submitted J. Phys. D
- [20] Vale C J, Upcroft B, Davis M J, Heckenberg N R and Rubinsztein-Dunlop H 2004 J. Phys. B: At. Mol. Opt. Phys. 37 29592967
- [21] Reichel J, Hansel W and Hansch T D 1999 Phys. Rev. Lett. 83 3398
- [22] Wang D, Lukin M and Demler E 2004 Phys. Rev. Lett. 92 076802